2013

Comparison of Gilmore-Akulichev equation and Rayleigh-Plesset equation on therapeutic ultrasound bubble cavitation

Zhong Hu
Iowa State University

Comparison of Gilmore-Akulichev equation and Rayleigh-Plesset equation on therapeutic ultrasound bubble cavitation

by

Zhong Hu

A thesis submitted to the graduate faculty

in partial fulfillment of the requirements for the degree of

MASTER OF SCIENCE

Major: Computer Engineering

Program of Study Committee:
Timothy A. Bigelow, Co-Major Professor
Joseph A. Zambreno, Co-Major Professor
Baskar Ganapathysubramanian

Iowa State University
Ames, Iowa
2013

TABLE OF CONTENTS

LIST OF FIGURES

LIST OF TABLES

ACKNOWLEDGEMENTS

First, I would like to thank my advisor Dr. Timothy Bigelow, who not only leads me into the exciting world of ultrasound therapy, but also inspires me how to do great research. With his generous help, I gradually figure out my own research picture beginning from a piece of white paper.

And also, I'd like to thank Dr. Joseph Zambreno for inspiring me to use GPU CUDA to speed up the bubble simulation process. Especially, the GPU cluster server, which he gives me access to, is essential hardware for me to finish the parallel computing part in my thesis.

In addition, I'd like to my dear friends and roommates, Zhuoru Wu and Kegeng Liu. They give me a lot of support throughout the whole two years. Without them, I wouldn't be that optimistic when facing hard financial situation.

Finally, great thanks to my parents who give me life and unconditional love.

ABSTRACT

The inertial cavitation of bubble clouds has been considered to be the hidden crucial mechanism for recent new therapeutic ultrasound applications such as Histotripsy and the ultrasound drug delivery. Although many models are already put forward to simulate the cavitation process, due to the inaccessible experimental validation, which model works closest to the real world situation is not well investigated. The objective of this thesis is mainly to compare the simulation performance of the popular Rayleigh-Plesset model and Gilmore-Akulichev model exposed to high intensity focused ultrasound in terms of the bubble equilibrium radius, the ultrasonic pressure, frequency and gas diffusion.

Our results show that under the same acoustic wave, before the first collapse, the bubble oscillates similarly with Rayleigh-Plesset and Gilmore-AKulichev models, but it collapses much more violently with Rayleigh-Plesset model. When more cycles of ultrasonic wave are exposed to the bubble, these two models behave disparately both in the oscillation and collapse stages. With Gilmore-Akulichev model, the bubble tends to oscillate in a more stable and bounded shape while it's expands and collapses unrealistically with Rayleigh-Plesset model. Also, the effect of the bubble gas diffusion is explored with Gilmore-Akulichev model. The gas diffusion is found to make the bubble expansion larger and collapse more dramatic, and this ability to sharpen curves tends to be stronger with higher pressure amplitude and lower frequency waves. Finally, GPU CUDA is implemented to simulate the

bubble cloud dynamics in Histotripsy via Gilmore-Akuchev model with gas diffusion taken into account. Compared to traditional CPU copulation, our CUDA simulation is proved to be 10X faster.

CHAPTER 1

INTRODUCTION

1.1 Therapeutic ultrasound overview

High power therapeutic ultrasound is gaining increasing attention for its potential in noninvasive therapy applications. Exposed to high frequency and high pressure, the acoustic energy will be deposited and transformed to the high temperature in the focused region to cause tissue necrosis and the proposed therapy based on this principle is called “HIFU” [1]. [2] finds that the acoustic wave also activates the microbubbles of the targeted region to nucleate, grow up and collapse in a short time, but whether the role the of bubble cavitation is beneficial or adverse hasn’t reached a consensus.

Alison [3] finds that the noninvasive thrombolysis can be realized by implementing the pulsed focused ultrasonic wave with frequency at 1 MHz and peak negative pressure at 12 *MPa* and this novel noninvasive tumor ablation modality is called Histotripsy. Different from HIFU, Histotripsy works as an invisible scalpel to ablate tumors mechanically without causing obviously heat effect. Later, T. L. Hall [4] reveals that nice real time ultrasound images can be collected while the Histotripsy is working to break down the tissue. This real time image feedback makes Histotripsy possible in clinical application if its ultrasound dosage is well designed.

Another new developing application of therapeutic ultrasound is in the drug delivery area [5]. Bubbles are first encapsulated with specific medicine, and then they function as the sender of the drug and flow with the blood current. When an interest location is reached, the focused ultrasound will work to collapse the bubbles in a short time to release the drug.

There're many other minimally invasive tumor ablation technologies such implementing radiofrequency waves [6], cryotherapy [7], lasers [8] and microwave energy [9]. Compared with the completely extracorporeal ultrasound modality, all of them may suffer with ionizing radiation, or leading to potential infection along with minimal intervention.

The inertial bubble cavitation is discovered in the HIFU application, and it is also believed to be the main mechanism for Histotripsy and the bubble enhanced drug delivery process. However, there's no well accepted model developed to simulate this mechanism though many candidate models are used in papers without validating their feasibility. The three most used models are GA (Gilmore-Akulichev) model [10][11], RP(Rayleigh-Plesset) model [12]and Herring model[13]. GA is originally developed for the testing of seismic airguns and underwater explosion application [10], and it's first applied by C.C. Church [11] to simulate the mechanism of the bubbles exposed to the extracorporeal shock wave used by Lithotripsy, which is a technique to break down the gallstone and kidney stones, and now it has been adopted to simulate the inertial cavitation of bubbles exposed to a high power mechanical waves. The RP (Rayleigh-Plesset) model describes the

dynamics of a free bubble in an incompressible fluid and assumes the velocity of the sound is infinite in the liquid. It is now the most widely used model to simulate the bubble dynamics in the bubble contrast agent in drug delivery area [14]. The Herring model [13] assumes a constant velocity of sound in the liquid and is a modification of the RP model. It's not used frequently in therapeutic ultrasonic application so it's not covered here.

Due to the complexity of the bubble dynamics itself when exposed to high pressure and high frequency ultrasound wave, selecting a good model to simulate this process is extremely important. Vokurka [15] compares the above three models and concluded that GA works better for large amplitude of bubble oscillations but the maximum normalized expansion ($\frac{R}{R_0}$) is confined to be between 1and 10, which is not applicable for the violent expansion situation in therapeutic ultrasound applications. V. Sboros [16] makes a comparison of RP and GA models with experiment validation and proves that RP is not feasible for simulating kinetics of contract agent bubbles in the bubble enhanced drug delivery application. The author carried out computations on shell coated bubbles at ~3 μm subjected to 3MHz sine wave. Kelsey [17] showed that the initial bubble radius would greatly affect the bubble response and optimal radius is a function of specific frequency and pressure amplitude in order to observe the maximum expansion, and therefore results in [16] are not sufficient to fully compare these models. Moreover, in contrast to the artificially coated bubbles in drug delivery area, the size of bubbles is randomly

distributed in Histotripsy, so a wide range of initial bubble radius needs been investigated in search for a feasible model for Histotripsy.

To our best knowledge, for ultrasound enhanced drug delivery application, although RP model is quite popular, its advantages over other models are not fully explored. And also, for the new Histotripsy therapy, there's no well recognized model to simulate the bubble activity. Therefore, in our project, in order to select an appropriate model to simulate the bubble dynamics in the Histotripsy background and discuss the reasonability of using RP model in the enhanced bubble drug delivery process, two models are compared in terms of the bubble response exposed to different ultrasonic frequency and pressure combinations. One point to notice is that, Church [11] compares the bubble response to the shock wave with gas diffusion concluded and the one without diffusion and proves that including gas diffusion is more desirable when bubble exposed to the shock wave. So in our comparison, whether including the gas diffusion in GA model is also covered.

1.2 GPU CUDA simulation for bubble clouds in Histotripsy

Bubble clouds, composed of violent interaction of thousands of bubbles, is observed in Histotripsy therapy and considered to be directly responsible for mechanically destroying the soft tissue at the focus [18]. Therefore, the simulation of the whole bubble cloud, excited by the high pressure and frequency is essential to understand the mechanism of Histotripsy. It's also significant for providing a standard reference to the ultrasound dosage for future clinical potential of

Histotripsy. In hence, the bubble cloud simulation is covered in the last part of our project. However, with large numbers of iteration operation inside the diffusion calculation, it takes long time to approach results in reasonable time. Also, the size of the cloud is usually in thousands, or even ten thousands of nanometer bubbles, so the computation time becomes a big bottleneck.

Nvidia CUDA is designed for general purpose parallel computing on GPU. Compared to other parallel platforms, it's cheap and easy to program. In our project, CUDA is applied to do the most computationally intensive task and proved to decrease the time as much as 10X compared to original sequential code written in C.

1.3 Thesis Organization

In Chapter 2, the mathematical models of RP and GA will be explained in detail, the numerical simulation method and simulation results will be demonstrated in Chapter 3. The parallel simulation of bubbles via GPU CUDA will be covered in Chapter 4. The last chapter will make a conclusion of my two year research and make a plan for future work.

CHAPTER 2

BUBBLE DYNAMICS AND SIMULATION MODELS

2.1 The bubble dynamics

Acoustic cavitation describes the response of bubbles exposed to the acoustic field. If the acoustic frequency is not large ($< 1\ MHz$) and the pressure amplitude much smaller than the ambient static pressure (≈ 101 KPa), the bubble will oscillate around its initial radius in a periodic mode. This is called stable cavitation and an empirical equation has been derived based on the simplified Keller-Herring model [17]:

$$R_0 \cong 3\ MHz\ um/f_0^{lin} \quad (1)$$

R_0 is the bubble radius in μm and f_0^{lin} is the acoustic frequency in Eq. (1).

However, with higher pressure level, the bubble response also largely depends on the pressure amplitude of the acoustic field, and thus Eq. (1) is no longer feasible in this "inertial cavitation" scenario.

Inertial cavitation involves the violent expansion and collapse of bubbles on the order of micrometer and even nanometer in a short time. In therapeutic ultrasound, inertial cavitation accelerates the heat effects of HIFU but may cause unwanted prefocal damage [19]; and also, it's already proved to be the major contributor for mechanical necrosis in Histotripsy [20] and drug delivery area [21]. Therefore either way, finding a reasonable model to simulate the inertial cavitation process accurately and reasonably is tremendously important to reveal the influence of inertial cavitation on the therapeutic ultrasound applications. RP and GA models are widely used in this situation and their

discussion will be detailed in 2.2 and 2.3. The efficacy of involving gas diffusion in the simulation is discussed in 2.4 and the acoustic field parameters are specified in 2.5.

2.2 Rayleigh-Plesset Model

The generalized Rayleigh-Plesset equation [12] describes the response of the bubble in the following form

$$\rho\left[R\frac{d^2R}{dt^2}+\frac{3}{2}\left(\frac{dR}{dt}\right)^2\right]=p_B-p_\infty-\frac{2\sigma}{R}-\frac{4\mu}{R}\frac{dR}{dt} \quad (2)$$

In Eq. (2), R is bubble radius, ρ is the density of the liquid where the bubble is and set to be water 998 g/cm^3; $p_B$is the pressure inside the bubble and p_∞ is the far-field pressure of the liquid surrounding the bubble; σ is surface tension, μ is fluid viscosity.

This model assumes single spherical bubble in an infinite medium, and the gas content of the bubble is constant.

2.3 Gilmore-Akulichev Model

Church [11] first implemented GA model into simulating the bubble response excited by the acoustic shock wave, and its basic form is

$$R\left(1-\frac{U}{C}\right)\frac{dU}{dt}+\frac{3}{2}\left(1-\frac{U}{3C}\right)U^2=\left(1-\frac{U}{C}\right)H+\frac{U}{C}(1-\frac{U}{C})R\frac{dH}{dR} \quad (3)$$

Where,

$$C=\sqrt{C_l+6H} \quad (4)$$

$$H=\int_{P_\infty}^{P(R)}\frac{dp_l}{\rho_l} \quad (5)$$

$$P(R)=p_g-\frac{2\sigma}{R}-\frac{4\mu_l U}{R} \quad (6)$$

In Eq. (3)(4)(5)(6), R represents the bubble radius, U is the bubble wall velocity, C is the acoustic speed at the bubble wall and H is the enthalpy. p_l is the liquid pressure, and the bubble wall pressure is P(R), p_g is the gas pressure inside the bubble, and μ_l is the liquid dynamic shear viscosity. The detailed derivation of Eq. (3)(4)(5)(6) is in [23].

Compared to RP model, the gas content of the spherical bubble is not necessarily constant. And this character makes possible to include gas diffusion in GA model.

2.4 Gas Diffusion

Gas diffusion happens when the gas densities of different media are different. More gas flows into the less gaseous area until their densities become identical. In our project, in the dilute bubbly liquid, with exposed high pressure acoustic wave, microbubbles are nucleated, expand and rupture and afterwards repeat the above process. During nucleation and expansion stage, gas would flow from the surrounding fluid to the bubble, whereas, during collapse stage, large amount of gas would be released from the bubble to the fluid.

With diffusion concerned, the gas pressure of p_g in Eq. (6) is no longer a constant value. Instead, it depends on the gas moles and the ever-changing bubble radius as shown in Eq. (7).

$$p_g = \left(P_0 + \frac{2\sigma}{R_0}\right)\frac{m}{m_0}\left(\frac{R_0}{R}\right)^{3\eta}\left(\frac{R_{0n}}{R_0}\right)^{3(\eta-1)} \qquad (7)$$

In Eq. (7), R_0 is the initial equilibrium radius and R_{0n} is the time-varying equilibrium bubble radius. m_0 is the initial number of gas moles and η is the gas polytropic exponent and its typical value is 1.4. To investigate the effect of gas diffusion on the inertial

cavitation, it will be added to the GA model to compare the bubble response with the one without gas diffusion included.

2.5 Acoustic Parameter Metrics

Kelsey J.C [17] derives the optimal initial bubble radius for maximum expansion depending on the acoustic frequency and pressure amplitude:

$$R_{optimal}=\frac{1}{\sqrt{0.0327f^2+0.0679*f+16.5P^2}} \quad (8)$$

In Eq. (8), P is the pressure amplitude for the acoustic sine wave in MPa. f and $R_{optimal}$ are frequency and initial optimal bubble radius in *MHz* and μm respectively.

For example, if f=1 *MHz*, P=1 *MPa*, then the optimal bubble radius is 0.2454 μm.

In order to get the best performance in our model, a wide range of frequency and pressure are included and the initial radius given to the model are calculated based on Eq. (4). Besides the acoustic frequency and pressure, the parameter PRF (Pulse Repetition Frequency) also affects the response of bubbles in Histotripsy. The PRF is much smaller than the acoustic frequency (the ratio is closed to ≈1:1000 in [22]). After the first several collapse cycles, with long time waiting for next excitation, the bubble would be fragmented into small nuclei and the old ones are not available. Therefore, instead of including PRF, a large range of initial bubble radii calculated via Eq. 4 are provided representing different starting radii generated in pulsed Histotripsy treatment.

Table 1 covers the range of frequency (in *MHz*), pressure amplitudes (in *MPa*) and radii (in μm) used in the simulation. Notice that when f=0.5 *MHz*, and pressure 8.0 *MPa*, the initial radius can be as small as 30.75 *nm*.

Table 1 The acoustic parameter metrics

P/*MPa* / f/*MHz*	0.01	0.1	0.3	0.5	0.7	1.0	3.0	5.0	8.0
0.5	4.7795	2.19727	0.8092	0.4899	0.3508	0.2459	0.0820	0.0492	0.03078
1.0	3.1273	1.9404	0.7942	0.4865	0.3495	0.2454	0.0820	0.0492	0.03077
3.0	1.4147	1.2281	0.7101	0.4651	0.3413	0.2425	0.0819	0.0492	0.03076
5.0	0.9290	0.8697	0.6152	0.4351	0.3289	0.2380	0.0817	0.0492	0.03075

The interaction of bubbles is also involved in the tissue destruction and the drug delivery process. And also in the drug delivery area, the bubble will be normally coated with a shell to keep its stability [24]. However, since our main goal is just to focus on the initial stage of single free gas bubble activity, both the shell and the interaction process are neglected in the simulation. The parameters describing the bubble response include the normalized bubble radius $\frac{R(t)}{R_0}$, the maximum expansion time $t_{R_{max}}$, and the collapse velocity V_{min}.

CHAPTER 3

SIMULATION RESULTS

For applications like the drug delivery, once the bubble undergoes its initial expansion and collapse, the shell will be ruptured and the drug will be released . So in Section 3.1only the first bubble expansion and collapse is considered in this scenario. For other applications like Histotripsy, multiple continuous acoustic cycles are expected in one pulse repetition period, so the bubble activity along 20 cycles of ultrasonic wave is discussed in Section 3.2. The stability of these two models would be covered in Section 3.3.

3.1 Bubble first collapse activity

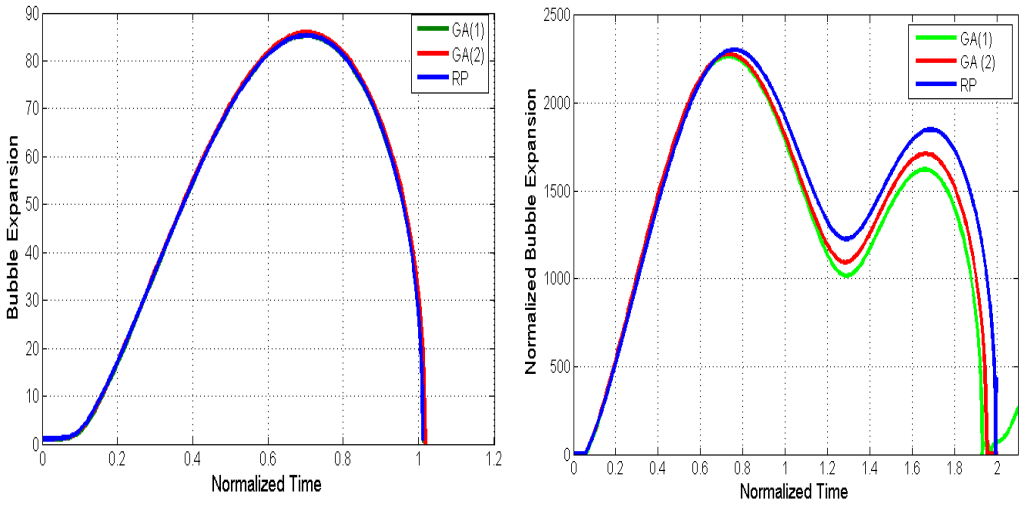

(a) **(b)**

Fig. 1 The normalized bubble expansion with the time cycle at frequency 0.5 *MHz*, pressure amplitude 10*KPa* (a) and frequency 5 *MHz*, pressure amplitude 8 *MPa* (b). The legend GA(1) is GA model without gas diffusion, and GA(2) is GA model where the gas diffusion is included.

During the first collapse from Fig. 1, when the frequency is at 0.5 *MHz* and pressure at 10 *KPa*, the bubble expansion tendency for different models are similar, but as the frequency increases to 5 *MHz* and pressure at 8 *MPa*, the specific expansion extent and maximum expansion time are becoming different for different models. Fig. 2 further explores the above differences. When the pressure amplitude is larger and the frequency smaller, the expansion extent will be maximized. Notice that when the pressure is larger than 1Mpa, regardless of the frequency, the expansion extent from Rayleigh-Plesset model is more dramatic than the other two. Fig. 2 also shows the differences in the maximum expansion time normalized with respect to the pressure amplitude. It indicates that for our frequency and pressure range, the maximum expansion happens within 2 cycles, which means that if maximum expansion is expected, 2-cycle acoustic wave works better than the single cycle one when other parameters are the same. And also, when the frequency is smaller and pressure larger, the maximum expansion would happen at a later time slot.

(a1) **(b1)**

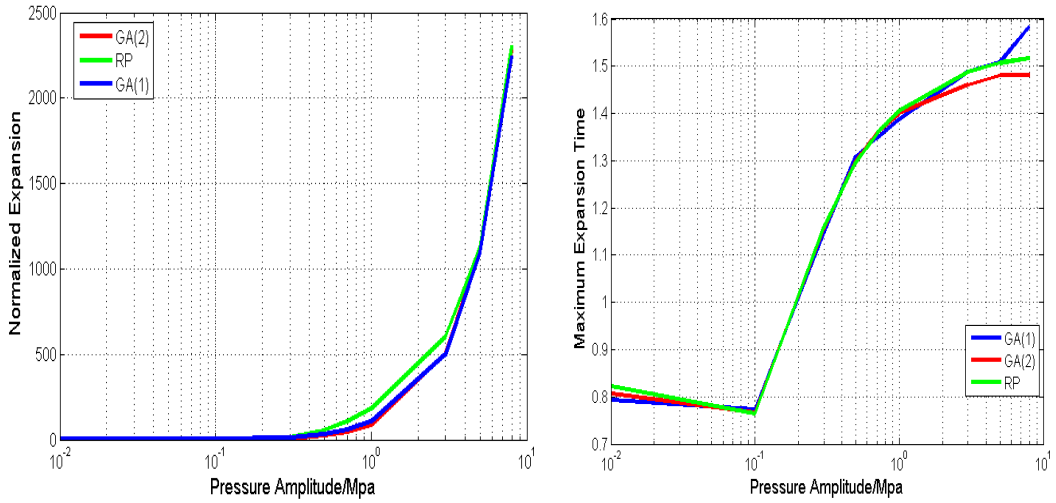

(a2)

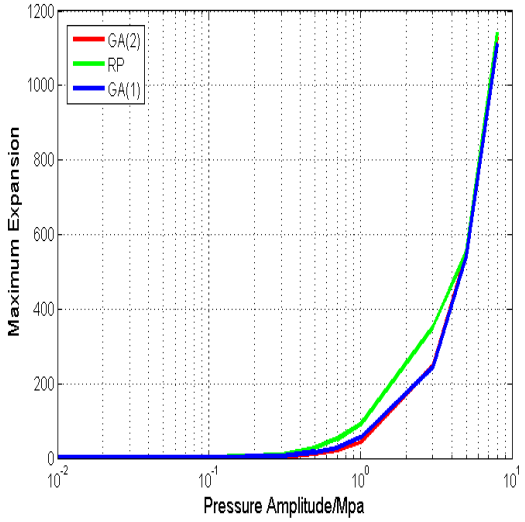
GA(2)
RP
GA(1)
Maximum Expansion
Pressure Amplitude/Mpa

(b2)

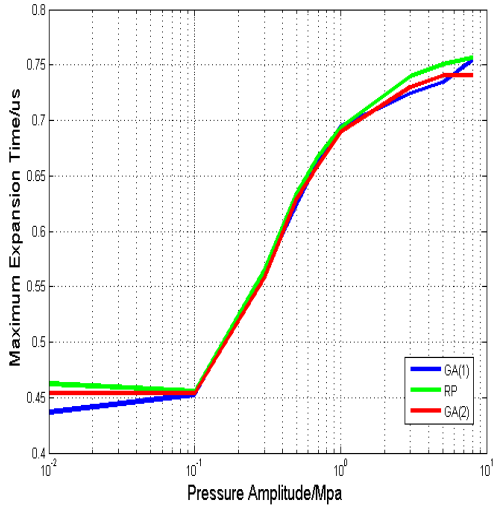
Maximum Expansion Time/us
GA(1)
RP
GA(2)
Pressure Amplitude/Mpa

(a3)

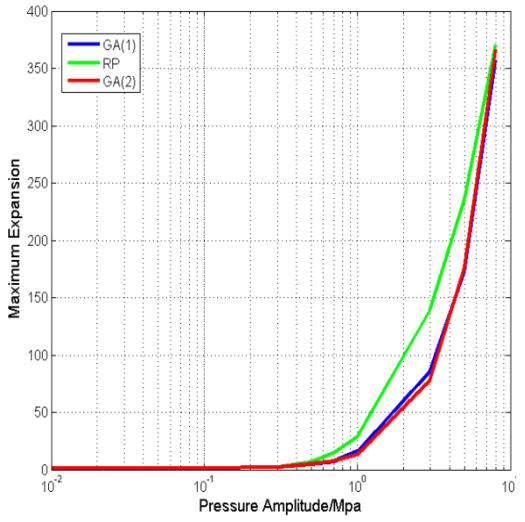
GA(1)
RP
GA(2)
Maximum Expansion
Pressure Amplitude/Mpa

(b3)

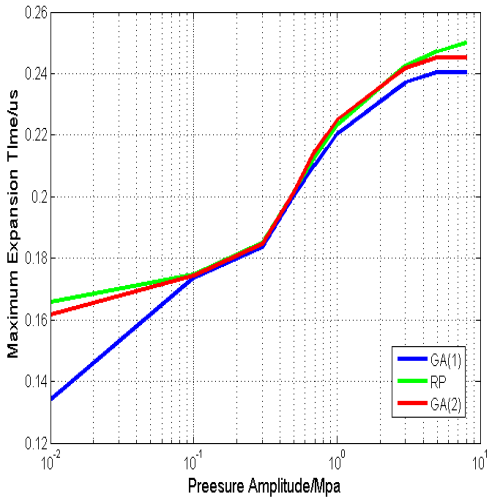
Maximum Expansion TIme/us
GA(1)
RP
GA(2)
Preesure Amplitude/Mpa

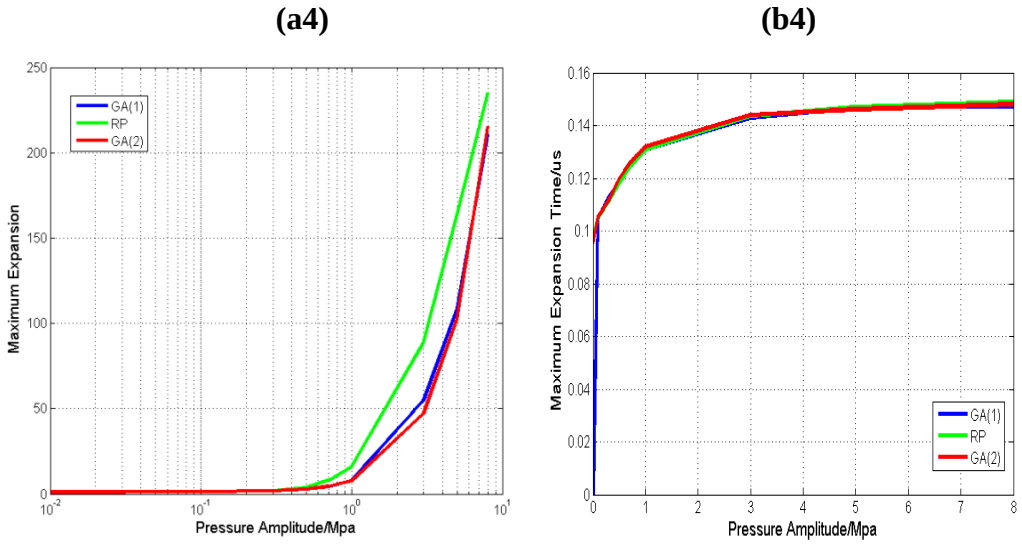

Fig. 2 The normalized maximum bubble expansion value (a) and time (b) with changing pressure amplitude when frequency is 0.5 MHz(a1,b1), 1MHz(a2,b2),3 MHz(a3,b3) and 5 MHz(a4,b4). The legend GA(1) is GA model without gas diffusion, and GA(2) is GA model where the gas diffusion is included.

When frequency is 0.5 MHz and pressure at 8 MPa as illustrated in Table 2, the maximum expansion for different models can be ~2000 within the first expansion. But the maximum velocity for RP can be as fast as 4690.7 Km/s while for the other two, it can only be ~1000 m/s. This indicates that the bubble collapses much more violently in RP model than in GA model although they have same maximum radius expansion extent.

Table 2, bubble first collapse time, velocity and maxim expansion when frequency is 0.5 *MHz* and pressure 8 *MPa*.

Models	Maximum Expansion	Maximum Expansion Time/us	Collapse Velocity (m/s)
Rayleigh-Plesset	2304.3602	0.80	4.6907exp(6)
Gilmore-Akulichev	2266.2061	0.396	841.094
Gilmore Akulichev-no Diffusion	2279.653	0.78	1157.97

3.2 Bubble activity within 20 Cycles

Fig. 3 below describes the bubble activity along 20 cycles, and it shows a much different scenario compared to Section 3.1. After the first expansion, the bubble goes remarkably different with RP and GA model.

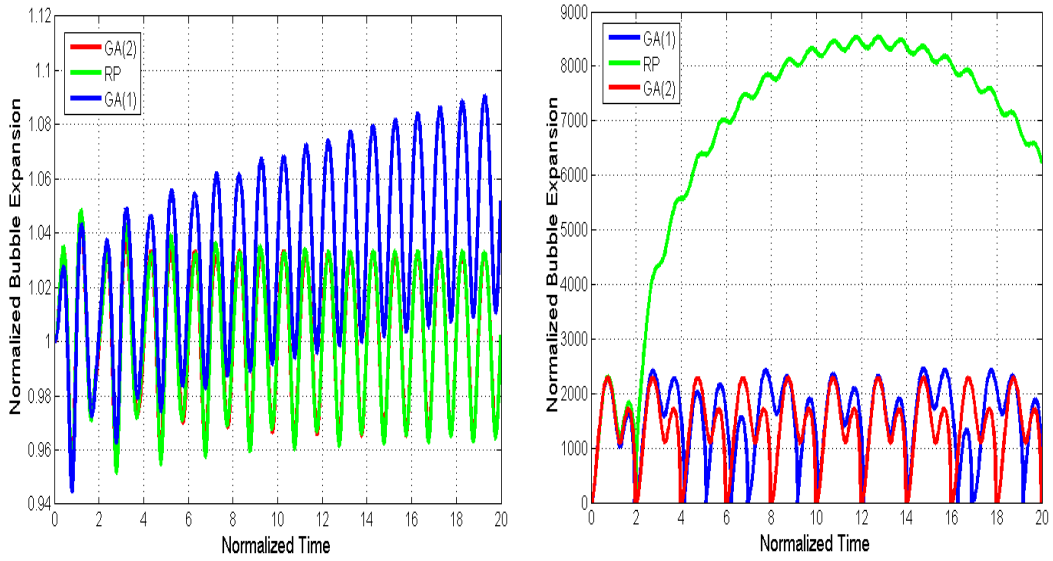

(a) (b)

Fig. 3 The normalized bubble expansion with the time cycle at frequency 0.5 *MHz*, pressure amplitude 300*KPa* (a) and frequency 5 *MHz*, pressure amplitude 8 *MPa* (b). The legend GA(1) is GA model without gas diffusion, and GA(2) is GA model where the gas diffusion is included.

Seen from Fig. 4, in spite of frequency, at small pressure (<1*MPa*), the maximum expansion is still similar, although specific bubble activity along time are different shown in Fig. 3.When the pressure is larger than 1 *MPa*, the maximum expansion becomes far more violent with RP model than the other two. The normalized maximum expansion can be 8533 and collapse velocity can be 1.0021exp (+18) m/s based on Table 3. This velocity obviously violates the special relativity theory that no matter can travel faster than the speed of light (~3exp(8) m/s)) in physical world. In lithotripsy where the shock

wave pressure amplitude can be 1GPa, the collapse velocity can only be $O(1000)$. Therefore, if a long time simulation is expected, Rayleigh-Plesset model is inferior to the other two.

Also, the effect of gas diffusion becomes more phenomenal in Fig.3(b). After first expansion, the bubble with gas diffusion tends to magnify both the expansion and collapse extent, causing the change more extreme. Fig.(4) further confirms this by observing that the maximum expansion with gas diffusion included is larger than the one without diffusion when the pressure amplitude is larger than 1 *MPa*. This makes sense in theory because during the expansion period, more gas are transferred into bubble, making the expansion extent larger than the one without diffusion considered; and during collapse, the gas released from the bubble could make the bubble even smaller.

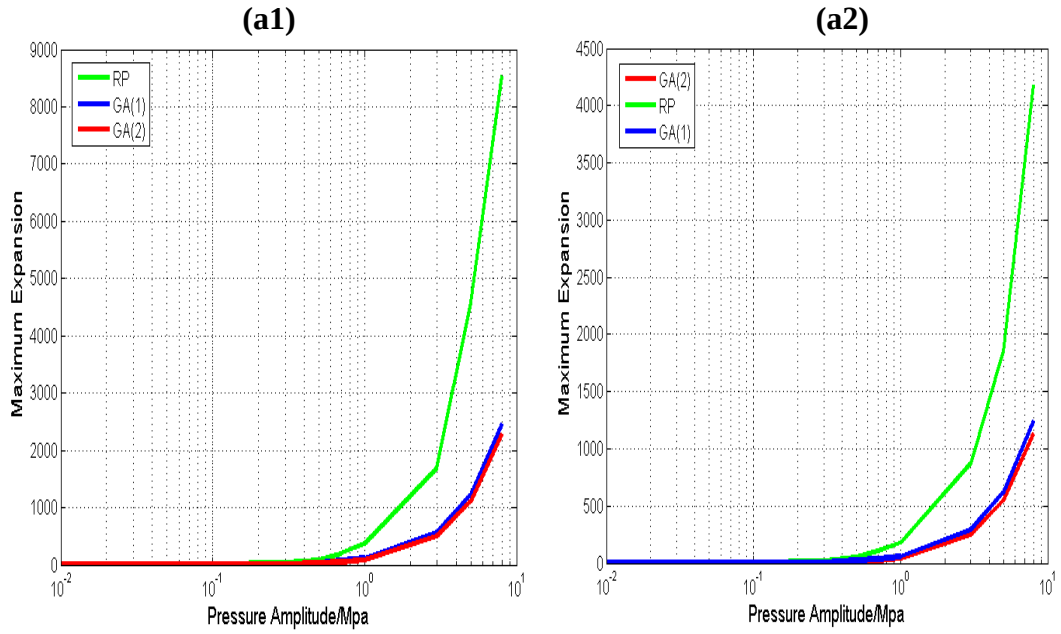

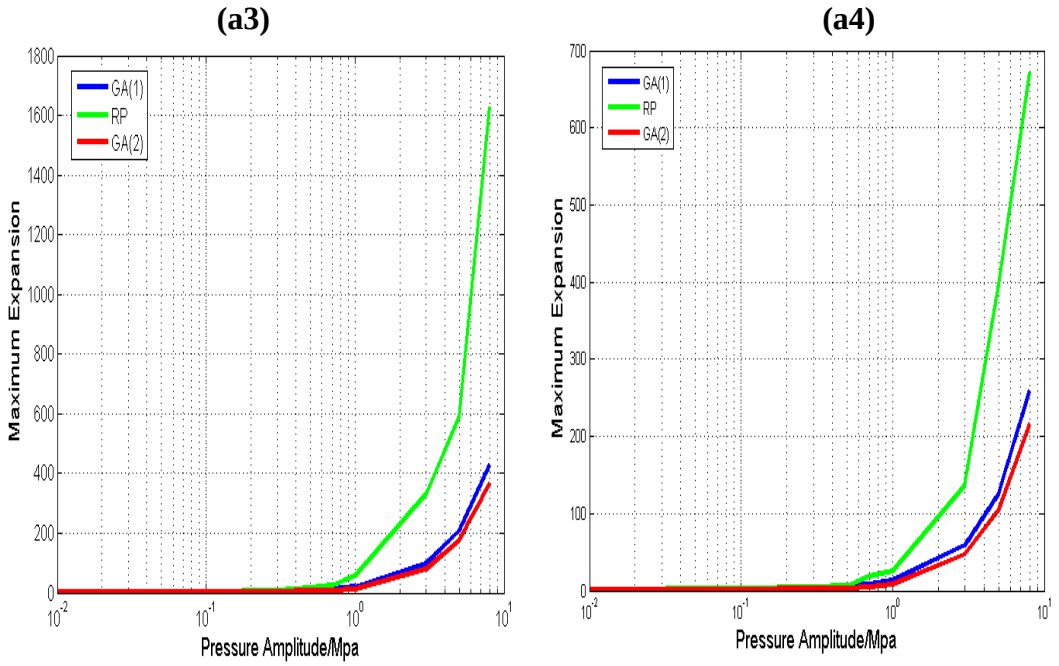

Fig. 4 The maximum bubble expansion value with changing pressure amplitude when frequency is 0.5 *MHz* (a1), 1*MHz* (a2), 3 *MHz* (a3) and 5 *MHz* (a4) The legend GA(1) is GA model without gas diffusion, and GA(2) is GA model where the gas diffusion is included.

Table 3, bubble maximum expansion value and time, and collapse velocity in 20 cycles when frequency is 0.5 *MHz* and pressure 8 *MPa*.

Models	Maximum Expansion	Maximum Expansion Time/μs	Collapse Velocity m /sec
Rayleigh-Plesset	8533.336	25.488	1.0021e+18
Gilmore-Akulichev	2458.151	29.7591	2446.52
Gilmore Akulichev-no Diffusion	2279.6530	1.4800	1556.89

3.3 Bubble activity in the last five average cycles

In order to verify the stability of bubble activity via different models along the time, the last 5 cycles are extracted from the whole 20 cycles. The average maximum expansion for each cycle and the standard deviation are calculated and plotted in Fig. 5.

(a1) (a2)

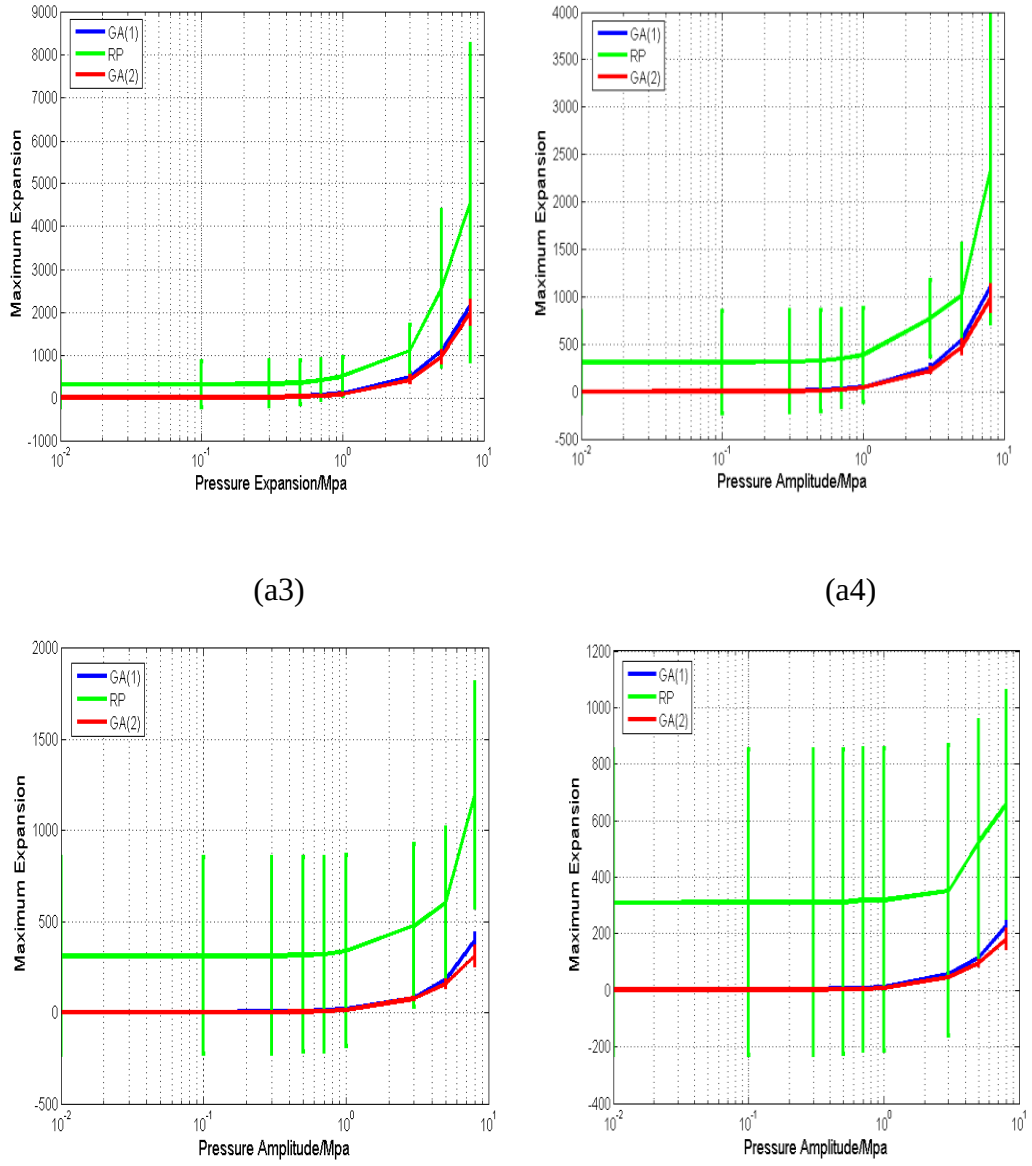

(a3) (a4)

Fig. 5 The average maximum bubble expansion value with changing pressure amplitudes when frequency is 0.5 *MHz* (a1), 1*MHz* (a2), 3 *MHz* (a3) and 5 *MHz* (a4). The legend GA(1) is GA model without gas diffusion, and GA(2) is GA model where the gas diffusion is included.

Fig.(5) reveals that for the last five cycles, GA model performs much more stable than RP. The modeling result of this characteristic determines whether Histotripsy can be considered as a reliable and well controlled modality for clinical application. In theory, since the second order term is included in GA, GA is assumed to be a more accurate one than RP. But still, experimental validity is yet needed urgently to further prove this.

CHAPTER 4

BUBBLE CLOUD SIMULATION VIA GPU CUDA

The bubble cloud is a direct boost to mechanically fractionating soft tissues in Histotripsy. Therefore, in order to pave the way for the future clinical application of Histotripsy, simulating the bubble cloud would provide a good reference for treatment planning and dosage design in advance.

[25] observes that in targeted region, the bubble cloud is generated and grow toward the source of acoustic wave very fast. The cloud is composed of thousands of microbubbles and each of them grows, expands, interacts and collapses. These bubbles are assumed to be independent from each other in dilute fluid and this indicates the potential of implementing the simulation via parallel tools. The high power acoustic wave utilized in Histotripsy is emitted originally in the form of sine wave. However, when crossing the boundaries of media with different acoustic impedance characteristics, the sine wave will be distorted and becomes nonlinear. KZK[26] is selected in our project to simulate the distorted acoustic wave applied to the bubble cloud. With analysis in Chapter 3, the significant effect of gas diffusion on the bubble expansion exposed to continuous acoustic wave is proved. Therefore, in order to get results as accurate as possible, gas diffusion will also be taken into consideration in spite of its slow computation speed. All the above requirements make the simulation of cloud bubble hard to finish in reasonable time. Therefore in our project, GPU CUDA will be used as the parallel computing tool.

4.1 GPU CUDA overview

CUDA, short for Compute Unified Device Architecture, is an emerging parallel programming model implemented on Nvidia GPU (Graphics Processing Units) [27]. Because of its easy programming and cheap compute cost, it has been widely used as a powerful scientific computing tool in molecular dynamics simulation [28], fast genome alignment [29] and so forth.

In our project, due to the high parallelism potential among thousands of bubbles inside one cloud, CUDA is introduced to model one bubble cloud and proved to increase the simulation speed by10X compared to running the same code in C++.

4.2 The acoustic source

To get a nonlinear acoustic wave model, KZK equation, modified based on Burgers equation, is used to simulate the wave source with consideration of specific location, non-linearity, and gas diffraction. In this equation, for bubbles in various locations, its incoming ultrasound wave is different. GA will be used as the simulation model for the activity of each bubble since it's confirmed to be a better simulation model in Chapter 3.

The KZK equation is:

$$\frac{\partial^2 P}{\partial z \partial \tau} = \frac{c_0}{2}\nabla_{\perp}^2 p + \frac{\delta}{2{c_0}^2}\frac{\partial^3}{\partial \tau^3} + \frac{\beta}{2\rho_0 c_0^3}\frac{\partial^2 p^2}{\partial \tau^2} \qquad (5)$$

P is the pressure amplitude; z is the axial coordinate of the wave; c_0 is the wave speed traveled in the medium; β is the nonlinearity coefficient; p_0 is the ambient density; δ is the sound diffusivity, and τ is the retarded time. Thank Dr. Joshua Soneson at FDA for sharing the code to KZK equations for spherically focused transducers and Jin Xu [24] for further verifying the correctness of this method used in Histotripsy.

4.3 Parallel model

Fig. 6 is the memory model of GPU and computation model for CUDA. The smallest compute unit in GPU is called thread. Thousands of threads form a block and within one block, a shared memory is used to store shared variables and data. In our project, each bubble, located in different places, is exposed to its specific acoustic pressure $p(x, y, z, t)$, so the simplest method is to assign each bubble to one thread in CUDA.

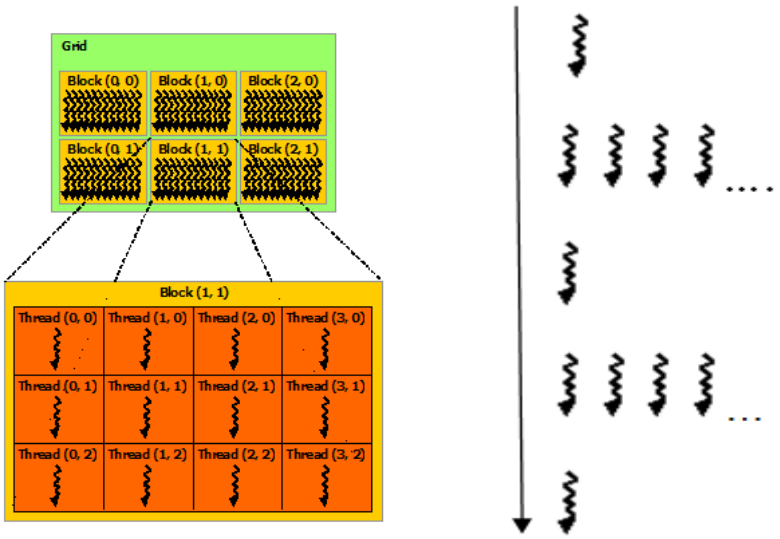

Memory model **Computation Model**

Fig .6 CUDA heterogeneous programming model [30]

The detailed flow chart is as following:

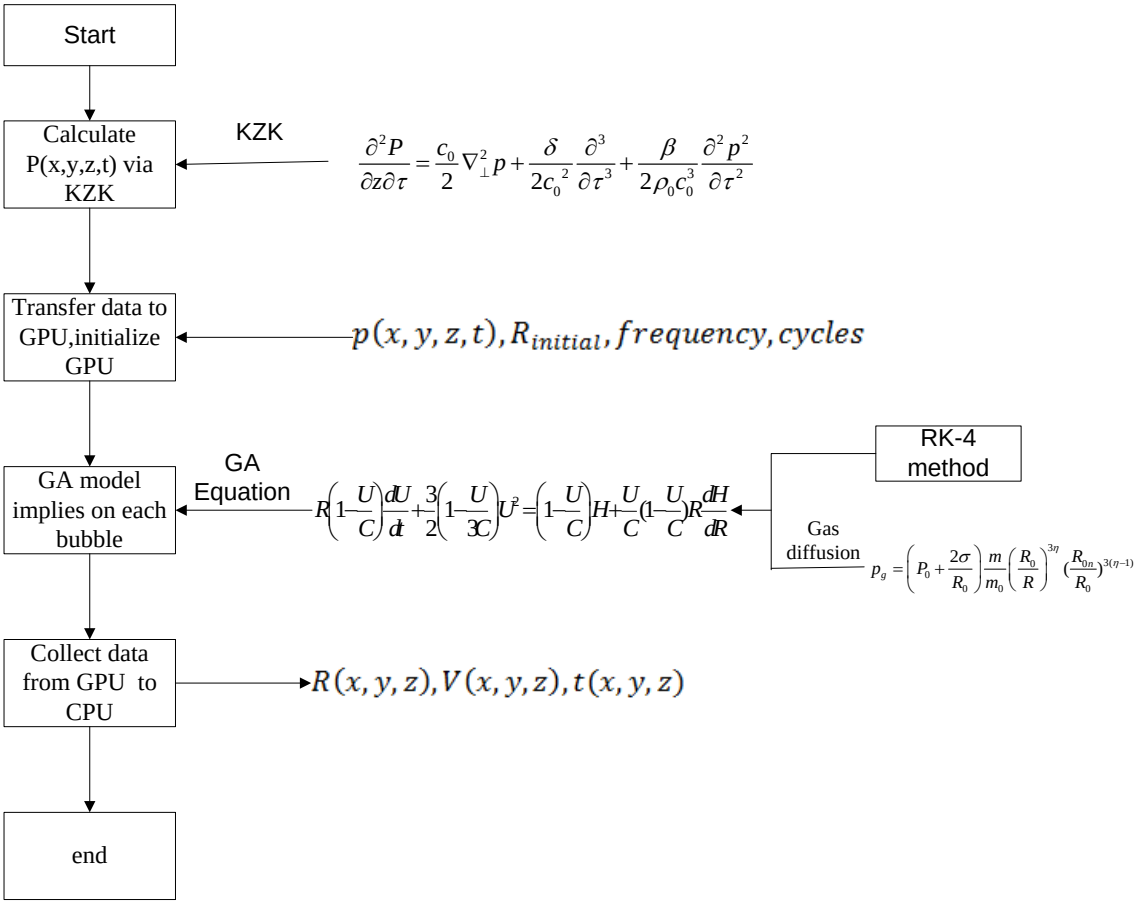

Fig. 7 The flow chart of the parallel cloud simulation

4.4 Comparison

The Nvidia GPU device we used is Quadro FX 5800, with 240 processing nodes and support for floating point calculation. The Host CPU is Intel Core 2 Duo E8400 with main frequency 3MHz. To compare the computing performance fairly, we also implement the same algorithm in C++ based on the above flow chart on the CPU. The performance difference is shown in table 4 and Fig. 8. The runtime is achieved based on the average time from 5 trials for each situation. At first, when the bubble number is smaller than 50, C++ performs better than CUDA, which makes sense because (1): the data transfer between GPU and CPU consumes time and (2) the bandwidth of GPU is

much smaller than CPU, and (3) the computation speed of CPU is faster than tens of concurrent threads. If bubble number is larger than 50, the advantage of computing on GPU becomes apparent and CPU works much slower than GPU with more bubbles. And also, when the bubble number doubles roughly (330, 825, 1815), CUDA runtime doesn't change linearly with the increase of bubble number whereas the C++ runtime does. The encouraging results open a new door for the future cloud simulation when more factors are included.

Table 4 the computation time comparison of CUDA and C++ in terms of the number of bubbles in one cloud.

Bubble numbers	CUDA runtime/s	C++ runtime/s
10	4136	758
50	5655	3361
330	8074	11089
825	8379	>30600
1815	11082	>109313

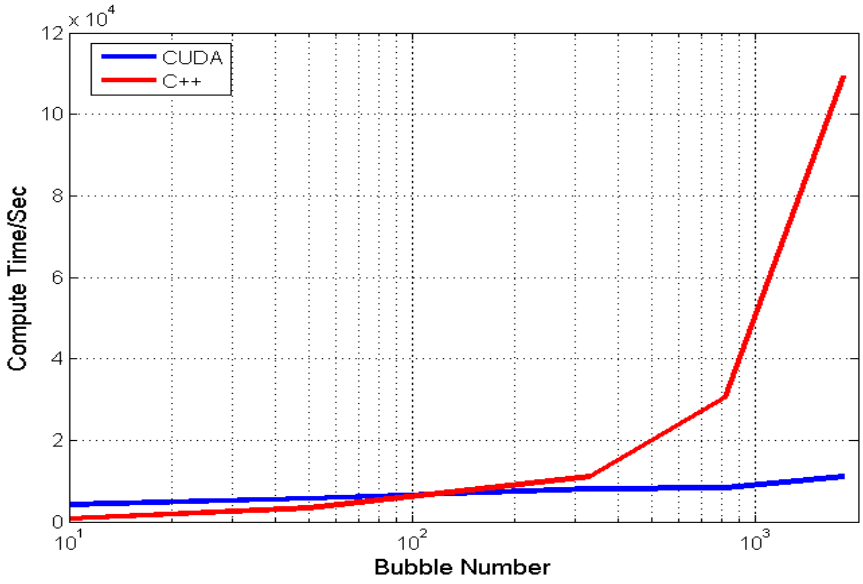

Fig. 8 the performance comparison of CUDA and C++ in terms of changing bubble number

CHAPTER 5

DISCUSSION AND FUTURE WORK

In our project, the classical models for inertial cavitation bubble exposed to therapeutic ultrasound are simulated and compared in terms of different ultrasound exposure conditions. For the first collapse, the simulated bubble activity of both GA and RP shows similar evolutionary trend, except that the bubble collapse from RP model is more violent compared to the other. And also, when gas diffusion is added to the GA model, the effect is not obvious for the first collapse. However, when 20 cycles are applied , results from RP model become greatly different from the other two, and the maximum velocity can even larger than the speed of light. The gas diffusion tends to flatten the sharp slope and constrain the extreme velocity change, making the simulation of GA more stable than the one without diffusion.

The computation intensive bubble cloud is the primary mechanism behind Histotripsy and many other ultrasound therapies. Based on the Gilmore-Akulichev model for each bubble, a bubble cloud model is built up and the computation efficiency is improved by 10X compared to C++ code via using GPU CUDA. However, this parallelism is still brute-force method and for each bubble, the iteration process induced by Runge-Kutta method and the gas diffusion process is the most time consuming part and they’re not parallelized internally yet. And also, the bubble interaction process is not included in our cloud model. Our next step is to incorporate the interaction activity between bubbles into our whole code and further parallelize the whole code to make it faster. Notice that in our parallel model, the initial bubble radius is constant and on the order of micrometer, while

the initial optimal bubble radius can be derived by [17] if the acoustic wave is linear and no gas diffusion there. Our future work will also involve finding the optimal initial radius when the wave is nonlinear and gas diffusion is included.

REFERENCES

[1] Kennedy JE. High-intensity focused ultrasound in the treatment of solid tumors, Nature Reviews Cancer, 2005, Vol. 5, Issue 4, April 2005, Page 321-327.

[2] C.C. Coussios, C.H. Farny, G.Ter Haar, R. A. Roy. Role of acoustic cavitation in the delivery and monitoring of cancer treatment by high-intensity focused ultrasound (HIFU), International Journal of Hyperthermia, 2007, Vol. 23, No. 2, Page 105-120

[3] Alison M. Lake, Timothy L. Hall, Kathleen Kieran, J. Brian Fowlkes, Charles A-Cain, William W. Roberts. Histotripsy: Minimally Invasive Technology for Prostatic Tissue Ablation in an In Vivo Canine Model Urology, Volume 72, Issue 3, September 2008, Pages 682–686.

[4] Hall, T.L.; Fowlkes, J.B.; Cain, C.A., "Imaging feedback of tissue liquefaction (histotripsy) in ultrasound surgery," *Ultrasonics Symposium, 2005 IEEE* , vol.3, no., pp.1732,1734, 18-21 Sept. 2005

[5] Pitt, William G., Ghaleb A. Husseini, and Bryant J. Staples. "Ultrasonic drug delivery-a general review." *Expert opinion on drug delivery* 1.1 (2004): 37-56.

[6] S.Nahum Goldberg, Radiofrequency tumor ablation: principles and techniques, European Journal of Ultrasound, Volume 13, Issue 2, June 2001, Pages 129-147.

[7] Tara K. Sotsky, Thanjavur S. Ravikumar, Cryotherapy in the treatment of liver metastases from colorectal cancer, Seminars in Oncology, Volume 29, Issue 2, April 2002, Pages 183-191.

[8] Vogl, Thomas J., et al. "Colorectal Carcinoma Metastases in Liver: Laser-induced Interstitial Thermotherapy—Local Tumor Control Rate and Survival Data1." *Radiology* 230.2 (2004): 450-458.

[9] Shibata, Toshiya, et al. "Small Hepatocellular Carcinoma: Comparison of Radio-frequency Ablation and Percutaneous Microwave Coagulation Therapy1."*Radiology* 223.2 (2002): 331-337.

[10] Gimore,F., The growth or collapse of a spherical bubble in a viscous compressible liquid, Technical Report No.26-4, California Institute of Technology, 1952.

[11] Church, C. C., "A Theoretical Study of Cavitation Generated by an Extracorporeal Shock Wave Li- thotripter", J. Acoust. Soc. Am., Vol. 86, No. 1, pp. 215-227, 1986.

[12] Plesset MS. The dynamics of cavitation bubbles. *Journal of Applied Mechanics* (ASME) 1949; **16**:228–231.

[13] Herring,C.,Theory of the pulsations of the gas bubble produced by an underwater explosion , in Underwater Explosion Research: v.2, 1950., Officer of naval Research, Dept of Navy, 1949.

[14] Coussios, Constantin C., and Ronald A. Roy. "Applications of acoustics and cavitation to noninvasive therapy and drug delivery." *Annu. Rev. Fluid Mech.* 40 (2008): 395-420.

[15] Vokurka, K. "Comparison of Rayleigh's, Herring's, and Gilmore's models of gas bubbles." *Acta Acustica united with Acustica* 59.3 (1986): 214-219.

[16] Sboros, V., et al. "The dependence of ultrasound contrast agents backscatter on acoustic pressure: theory versus experiment." *Ultrasonics* 40.1 (2002): 579-583.

[17] Carvell, Kelsey J., and Timothy A. Bigelow. "Dependence of optimal seed bubble size on pressure amplitude at therapeutic pressure levels." *Ultrasonics*51.2 (2011): 115-122.

[18] Xu, Zhen, et al. "Evolution of bubble clouds induced by pulsed cavitational ultrasound therapy-histotripsy." *Ultrasonics, Ferroelectrics and Frequency Control, IEEE Transactions on* 55.5 (2008): 1122-1132.

[19] C. C. Coussios, C. H. Farny, G. Ter Haar, and R. A. Roy, "Role of acoustic cavitation in the delivery and monitoring of cancer treatment by high-intensity focused ultrasound (HIFU)," International Journal of Hyperthermia, vol. 23, pp. 105-120, 2007.

[20] Xu, Zhen, et al. "Controlled ultrasound tissue erosion: The role of dynamic interaction between insonation and microbubble activity." *The Journal of the Acoustical Society of America* 117 (2005): 424.

[21] Tezel, Ahmet, and Samir Mitragotri. "Interactions of inertial cavitation bubbles with stratum corneum lipid bilayers during low-frequency sonophoresis."*Biophysical journal* 85.6 (2003): 3502-3512.

[22] Xu, Zhen, et al. "Effects of acoustic parameters on bubble cloud dynamics in ultrasound tissue erosion (histotripsy)." *The Journal of the Acoustical Society of America* 122 (2007): 229.

[23] Klibanov, Alexander L. "Microbubble Contrast Agents." *Investigative Radiology*, 41.3 (2006): 354-362.

[24] Xu, Jin. "Mechanical Destruction of Biological Tissue by High Intensity Focused Ultrasound Histotripsy." Iowa State University, 2011.

[25] Xu, Zhen, et al. "Evolution of bubble clouds induced by pulsed cavitational ultrasound therapy-histotripsy." *Ultrasonics, Ferroelectrics and Frequency Control, IEEE Transactions on* 55.5 (2008): 1122-1132.

[26] Rozanova, Anna. "The Khokhlov–Zabolotskaya–Kuznetsov equation." *Comptes Rendus Mathematique* 344.5 (2007): 337-342.

[27] Owens, J.D.; Houston, M.; Luebke, D.; Green, S.; Stone, J.E.; Phillips, J.C., "GPU Computing," *Proceedings of the IEEE* , vol.96, no.5, pp.879,899, May 2008

[28] Anderson, Joshua A., Chris D. Lorenz, and Alex Travesset. "General purpose molecular dynamics simulations fully implemented on graphics processing units." *Journal of Computational Physics* 227.10 (2008): 5342-5359.

[29] Trapnell, Cole, and Michael C. Schatz. "Optimizing data intensive GPGPU computations for DNA sequence alignment." *Parallel Computing* 35.8 (2009): 429-440.

[30] Lindholm, E.; Nickolls, J.; Oberman, S.; Montrym, J., "NVIDIA Tesla: A Unified Graphics and Computing Architecture," *Micro, IEEE* , vol.28, no.2, pp.39,55, March-April 2008.

[31] Hazewinkel, Michiel, ed. (2001), "Runge-Kutta method", *Encyclopedia of Mathematics* , Springer

[32] Arciniega, Armando, and Edward Allen. "Rounding error in numerical solution of stochastic differential equations." (2003): 281-300.

[33] Higham, Nicholas J. *Accuracy and Stability of Numerical Algorithms. Society for Industrial and Applied Mathematics, Philadelphia, PA, USA, 2002*. ISBN 0-89871-521-0. xxx+ 680 pp, 1996.

[34] Higham, Nicholas J. "The accuracy of floating point summation." *SIAM Journal on Scientific Computing* 14.4 (1993): 783-799.

[35] Ilie, Silvana, Gustaf Söderlind, and Robert M. Corless. "Adaptivity and computational complexity in the numerical solution of ODEs." *Journal of Complexity* 24.3 (2008): 341-361.

[36] Bogacki, Przemyslaw, and Lawrence F. Shampine. "A 3 (2) pair of Runge-Kutta formulas." *Applied Mathematics Letters* 2.4 (1989): 321-325.

[37] Cash, Jeff R., and Alan H. Karp. "A variable order Runge-Kutta method for initial value problems with rapidly varying right-hand sides." *ACM Transactions on Mathematical Software (TOMS)* 16.3 (1990): 201-222.

[38] Dormand, John R., and Peter J. Prince. "A family of embedded Runge-Kutta formulae." *Journal of computational and applied mathematics* 6.1 (1980): 19-26.

APPENDIX

CONVERGENCE OF ADAPTIVE RK-4 METHOD

In theory, for the first order differential equation:

$$y' = f(x, y) \qquad (6)$$

If RK-4 is applied to solve Eq. (6) numerically, the truncation error ε_t would be $O(h^5)$ [31].

Obviously, $\lim_{h \to 0} O(h^5) = 0$, which means if the step size is set small enough, the ε_t could be minimized to zero finally. In real world, due to the limited approximation of real numbers in computer, instead of making ε_t to be zero, a realistic tolerant bound is set so that ideally if ε_t decreases monotonically and finally below the tolerant bound, then the step size is said to satisfy the convergence test and the corresponding result is trustable.

Therefore, initially in our project, we did the following experiment to search for a feasible step size to make the result convergent. The relative error bound here is arbitrarily chosen as $2 * 10^{-5}$. Given the rough maximum bubble radius can be O(1000), the bound guarantees a satisfying small difference.

The relative error is defined as

$$\varepsilon_n = \left| \frac{\max(R_{n+1}) - \max(R_n)}{\max(R_n)} \right|, \quad n \in \{1,2,3, \dots\} \qquad (7)$$

For solving GA with RK-4, the initial step size *h* is 5 *ns*, but it is found so large that the program crashes with invalid values. Only until *h* is around 10.9 *ps*, the steep region is traversed and valid values are reached. Seen from Fig. 9, 10.9 *ps* is already a small

enough step size to make the relative difference well below $2 * 10^{-5}$.However, with smaller step size given, the error doesn't decrease monotonically. Instead, it's changing randomly with the minimum error at the step size between 6.84 *ps* and 6.31 *ps*.

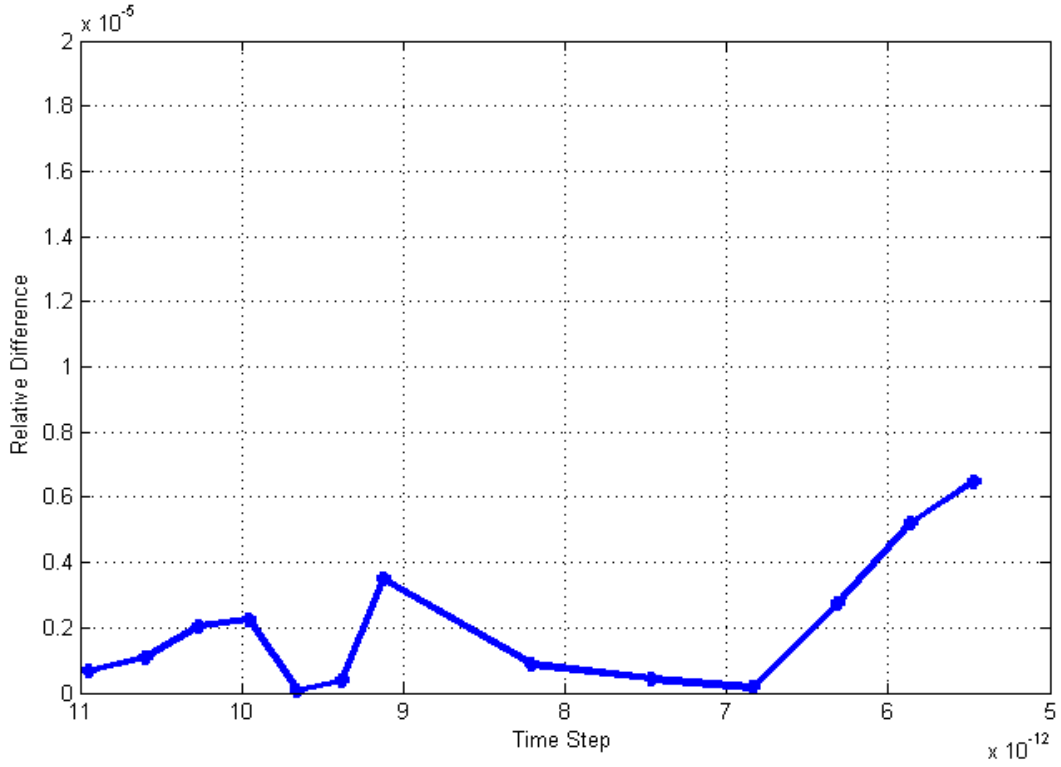

Fig. 9 The relative error change with different time step

Besides truncation error ε_t, the round off error will also be involved in numerical computation if the step size is too small. [32] does several the numerical experiments with Euler's method and shows that the rounding error is inversely proportional to $\sqrt{h}$ .For our computation, double precision Matlab is implemented, meaning the valid result is within 16 digits per step. With 20 cycles of 0.5 MHz sine wave exposed, the number of iteration is $O(10^6)$. Large iteration times and small step size not only make the computation more time-consuming, but also accumulates the round-off error to an extent which will lead to undesirable results eventually. This is probably why the error is

randomly changing along the way in Fig. 10. Another contributor may be from the rounding error during the iteration process. Small steps size indicates small change of radius for each iteration ($dR \approx O(10^{-16})$), and these small values are easily rounded, and this kind of error is more apparent just before the bubble expansion period. The radius iteration in that moment can be expressed as $R + dR = O(1000) + O(10^{-6}) \approx O(1000)$.

With the above reasons bearing in mind, three feasible approaches can be applied to reduce them. One is to directly increase the computation precision by adding some external software packages. Although the precision becomes higher, the corresponding computation time is much longer, as well. Another way is to implement some compensated methods like Kahan summation rule [33], pairwise summation [34] and so forth.

The last alternative is to implement adaptive step size adjustment strategy. Adaptive method has been used dominantly in current numerical simulation applications [33]. Compared to the traditional fixed method, the step size can be adjusted in real time based on the local error, with big step size for smooth region and small step size for sharp region. This approach will focus the most computation energy on the most remarkable region efficiently and accurately. The round-off error always exists in the computation. Whereas overall, the number of iteration could be largely reduced by thousands and even millions [35] if large step is applied in the preceding smooth region, and this could slow down the accumulation of round-off error and decrease its influence on the final result.

As shown in Fig. 1, the shape of the bubble radius expansion within the first expansion is increasing at the fist 0~1.8 cycles and only in the last moment, the bubble collapses in

a very fast speed. This is where the adaptive method could display its advantage to the full.

From step *n* to *n+1*, RK-4 method is used to discretize Eq.(6) as given:

$$y'_{n+1} = y_n + h\sum_{i=1}^{4} b'_i\, k_i \qquad (8)$$

$$y_{n+1} = y_n + h\sum_{i=1}^{4} b_i\, k_i \qquad (9)$$

y'_{n+1} is the estimate of y_{n+1}.

So the one step error is $\left|y_{n+1} - y'_{n+1}\right| = h\left|\sum_{i=1}^{4}(b_i - b'_i)\, k_i\right|$. There're variant ways to set the value of the weights b_i and b'_i [36][37][38]. To add some flexibility, Our project here simply identifies b_i and b'_i to be 1 and two local error indicators as following:

$$\varepsilon_{n+1}{}^{1} = |k_1 - k_2| + |k_2 - k_3| \qquad (10)$$

$$\varepsilon_{n+1}{}^{2} = \frac{|k_1 - k_2|}{|k_2 - k_3|} \qquad (11)$$

And these two indicators would be plugged in the classical RK-4 to adjust the step size in real time as shown in Fig. 10.

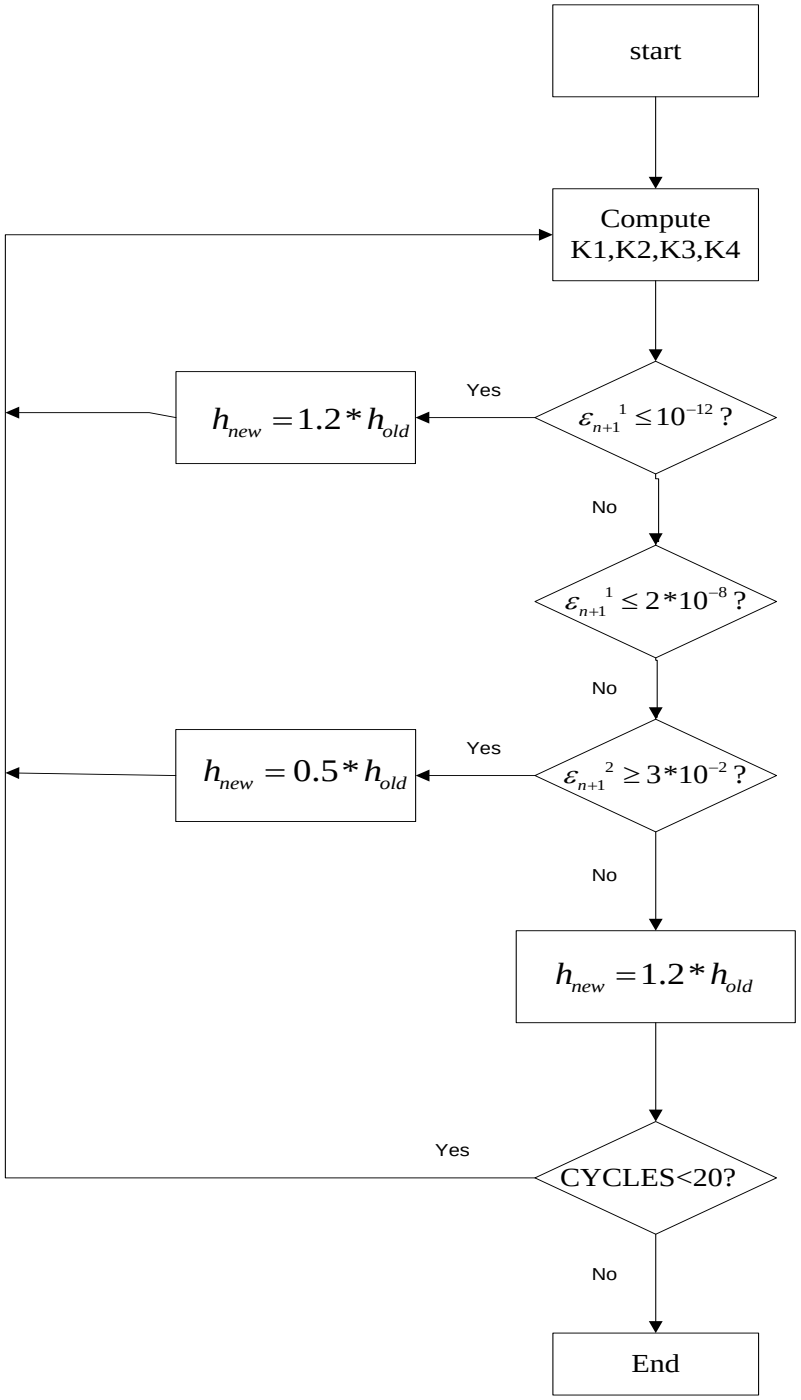

Fig. 10 The flow chart of Rk-4 with adaptive step size control

With the control in Fig. 11, the local error can be well controlled. The global error is defined as the accumulation of the local error along iteration:

$$\varepsilon_{global} = \sum_{i=i}^{n} \varepsilon_{local}^{i} \qquad (12)$$

Although two local error indicators are applied in our project, either way, the global error is well controlled as long as the number of iteration is finite.